



An Efficient and Reliable Method for Regional Analysis of Breast Thermographic Images

Mazhar B. Tayel¹, Azza M. Elbagoury^{2*}

¹Electrical Engineering Department, Faculty of Engineering, Alexandria University, Alexandria, Egypt

²Basic Science Department, Faculty of Engineering, Pharos University, Alexandria, Egypt

Abstract

Thermography is a promising screening technique for breast cancer diagnosis. It has many superiorities to make it a primary step towards early detection of breast cancer worldwide. Automated diagnosis of diseases become a vital tool in medicine. Segmentation is an essential step in classification and determination of region of interest (ROI) of thermographic images. The performance of deep machine learning networks has been making them an efficient end-to-end technique for computer vision applications. However, segmentation of images by the current deep neural networks suffers from a coarse segmentation boundary.

In this work, a deep learning framework is proposed utilizing a novel multi-path Convolutional Neural Network combined with multi-band of breast thermographic images as inputs to attain an augmented segmentation performance and also to refine the segmentation boundary. The non-subsampled contourlet transform for breast thermographic images is applied as a pre-processing stage. The proposed technology allows for optimal local and global contextual determination. Assessment of the proposed technique is based on a public breast infrared thermographic image database. The proposed model achieved higher accuracy, sensitivity, specificity, BF Score, and Jaccard index, even with small number of images. Also, certain improvement regarding visual assessment is accomplished without any post-processing compared with previous works.

Keywords

Breast Cancer, Thermographic image, Deep Learning, Fully convolutional neural network, Non-Subsampled Contourlet Transform, AlexNet.

1. Introduction

Breast cancer takes the first place for diagnosis in women among all incidence cancers and takes the second place in mortality among all cancer types. Many studies have concluded that detecting breast cancer in an early stage can significantly increase survival rates [1]. Mammography has been considered as the “gold standard” screening technique among various imaging modalities for early detection of breast tumors. Unfortunately, mammography has many limitations, such as cost, exposure to x-ray radiation harmful effects and compression of breast causes discomforts to the women. Also, the sensitivity of mammography depends on the physical nature and age of women. Moreover, mammogram is to be performed once every one or two years, during that cancer could progressively develop worse to higher grade.

Nowadays, breast thermography fills the insufficiency gap among other screening techniques. Thermography acts as a safe early risk marker of breast pathology [2], [3], [4]. Thermography has distinguished itself as the earliest breast cancer detection technology, and has the potentiality of detecting breast cancer 10 years earlier than traditional mammography [5], [6]. Also, unlike mammography which can detect the tumors only when its size exceeds a certain limit, thermography can even detect the small tumors where that regions contain a tumor are usually having a higher temperature when compared with the normal surrounding regions [7]. Also, thermography can yield better cancer detection performance in the case of dense breasts (breasts of young females) [8]. Thermography technique is less expensive than mammography and magnetic resonance imaging (MRI) techniques. Also breast thermography protocol is a non-invasive, non-ionizing, radiation-free, painless, contactless, quick and safe diagnostic procedure that needs minimal effort. Consequently, thermography is expected to be one of the most effective modalities for tumor early detection.

Many reviews had introduced several algorithms that extract ROI in breast thermographic images. Those algorithms were region-based, threshold-based, and edge-based techniques, including combination of some other methods, such as: borders detection, parabolic Hough transform, active contours, anisotropic filters and interpolation, k-means clustering and Hidden Markov Model [9]. Most of those works are semi-automatic or manual segmentation methods. However, The inherent amorphous characteristics of breast, absence of clear edges, low contrast, lack of clear limits of images and intensity inhomogeneity make segmentation a hard task. So, finding an accurate breast contour and extracting exact breast area by fully automatic technique is a challenging task. So, the tasks of machine learning (ML) can play a vital role to determining the local and global features derived from a proposed augmented segmentation methods.

2 . Objective

- I. Augment the data of available breast thermographic images.
- II. Determine the local and global features of the analyzed breast thermographic images.

3 . The Proposed Methodology

This work proposes a novel approach aims to tackle the existing intrinsic segmentation issue using the power of deep learning (DL). To obtain this goal, a multi-band multi-path (MBMP) fully convolutional network (FCN) is proposed which must has ability to extracting and learning both of local and global features. The proposed MBMP-FCN network consists of two paths based on the AlexNet-FCN, also each separate path must be trained on different bands of input thermographic images. The inputs to the proposed MBMP-FCN are the decompositions of the original breast thermographic images through a non-subsampled contourlet transform (NSCT) [10] as pre-processing stage, the NSCT grants the proposed model the trait of the multi bands.

The proposed MBMP-FCN structure model consists of three main stages: pre-processing stage that composed from a NSCT decomposition, convolution stage, and segmentation stage, as shown in Figure 1.

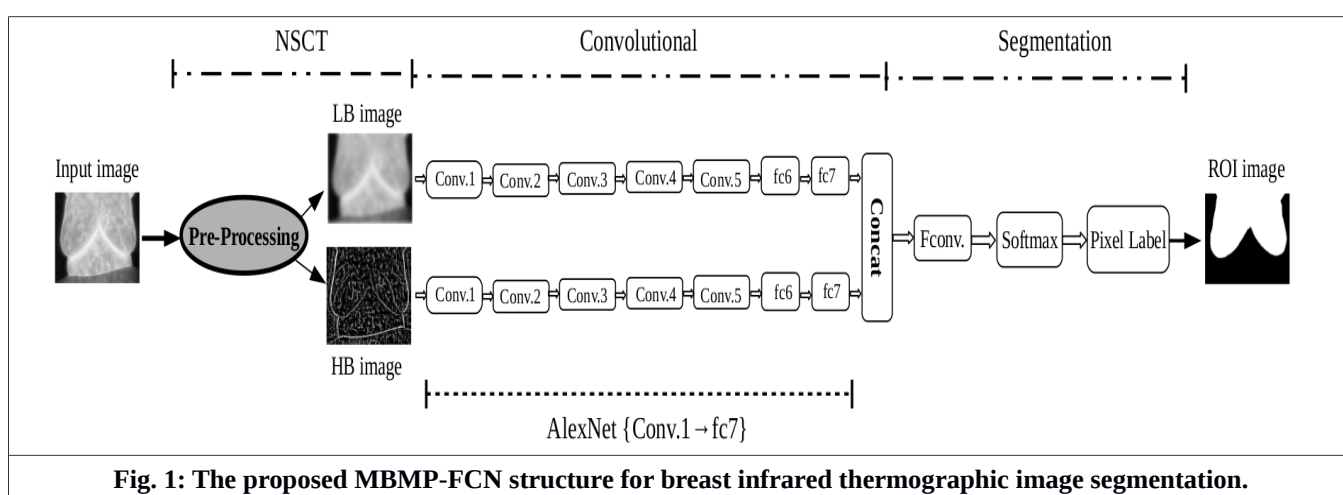


Fig. 1: The proposed MBMP-FCN structure for breast infrared thermographic image segmentation.

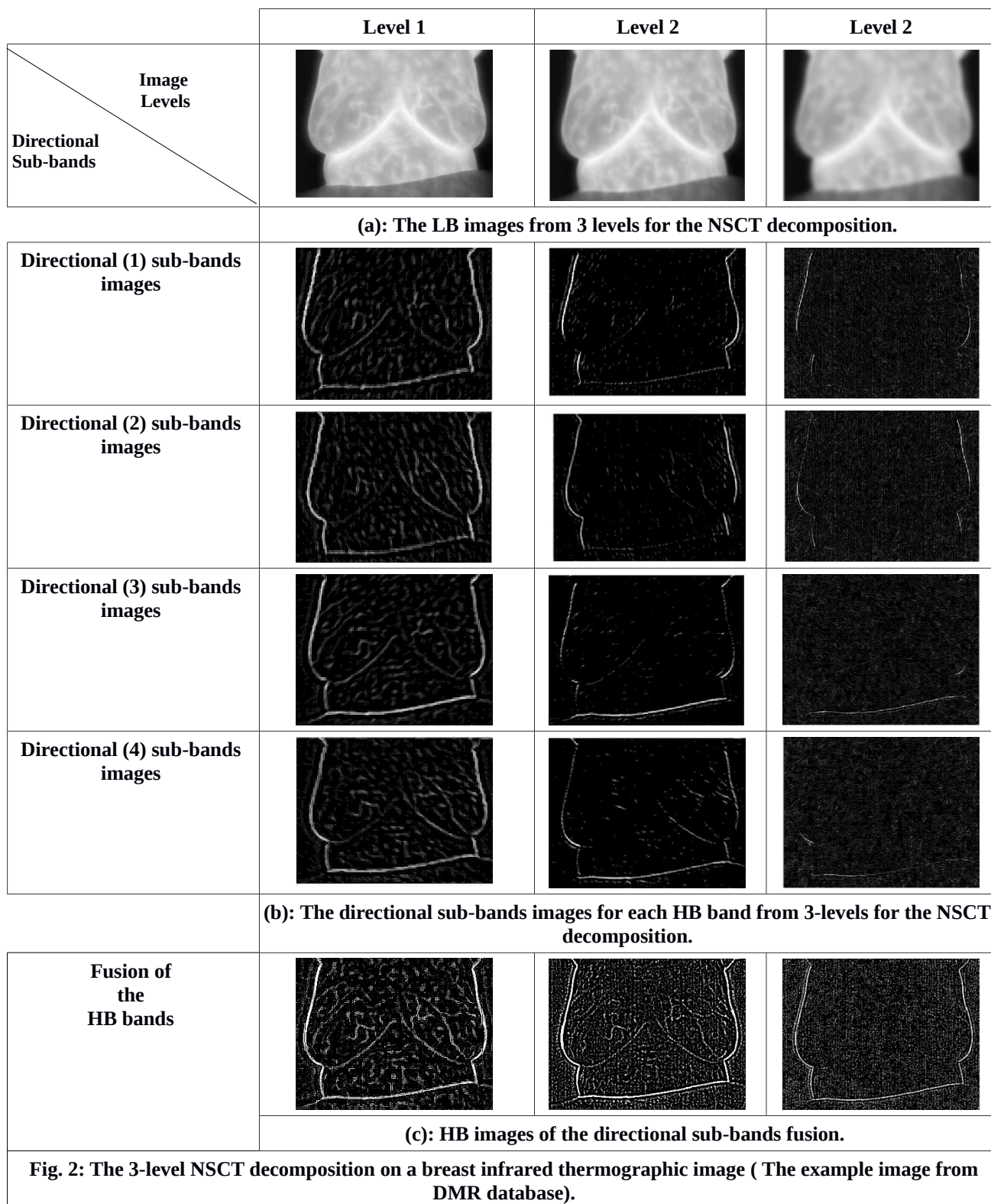
3.1. The Pre-processing stage

The input images are decomposed by the NSCT to increase image local and global representations. Introduction of the NSCT gives much detailed information about the smoothness of boundaries and edges of the image. Pyramid filter “pyrexc” and Directional filter “vk” are employed because of their good performance in feature extraction for medical images [10]. Also, the study shows that three-levels decomposition of the NSCT are sufficient applied for image segmentation. Each decomposition level is be augmented as follows: once the 1-level is utilized and the numbers of directional sub-bands (n) are set to two for all HB scales, there will be 4-directional sub-bands ($2^n = 2^2 = 4$) and one LB. Propagating consecutively via the 3-levels; each scale extracts both of the 4-directional sub-bands of HB and the one of LB.

Figure 2 shows the 3-levels of the NSCT decomposition, three images of the LB are shown in Figure 2 (a). Figure 2 (b) presents the directional sub-bands images for the HB bands at each level of decompositions.

The 4-directional HB images are fused to generate one HB image for the scales (1, 2 and 3). The images in a given column of Figure 2 (b) are fused to produce a corresponding images in Figure 2 (c). To generate a 3-channel format as the input for the LB path (first path), 3-copies of each HB image are concatenated along the third dimension. Similarly, three copies of each LB image are concatenated, which are employed as the 3-channel input of a HB path (second path). The three-channels of the image are employed based on the pre-trained FCN-AlexNet which supports 3-channels input images.

A glance at the different decomposition levels in Figure 2, distinctive features always exist and there is a clear trend concerning the capturing of contours, even though at the different scales. Furthermore, from Figure 2 (c), there is a clear observation concerning the contour features which are captured of HB images, however, the features become coarser with the increase of the decomposition level. In particular, it can be seen that the features captured at level 3 are becoming too coarse that only the main contours were extracted. Despite that, the distinctive features always exist and don’t disappear. Therefore, only the 3-levels of the NSCT are enough to decompose. As a consequence, the contours would be preserved smoothly for each image which is the useful features for the model.



3.2. The convolutional stage

Contains two parallel paths to accept the multi-bands of the NSCT. The two paths have the same architecture. Also, the two paths have hyper-parameters of the first seven layers of the FCN-AlexNet. Each path consists of a series of convolutional layers and max-pooling layers. In the beginning, the FCN-AlexNet is trained on the CamVid database [11]. The learned parameters of the pre-trained FCN-AlexNet are transferred and initialized to the two paths preparing for the fine-tuning process. The channels number of the LB and HB paths, separately, are emulating the RGB channels of the pre-trained FCN-AlexNet. That provides an opportunity for the proposed MBMP-FCN to take the full utilization from the pre-trained parameters of the FCN-AlexNet and transferring them without carrying out any shorthand for the first layers' parameters. Finally, the feature maps from each path are concatenated via a feature-level fusion. Also, merging features from various bands' levels helps to capture a high level of full semantic/contextual information; local and

global. Then "the concatenated feature map" is propagated to the successive layers.

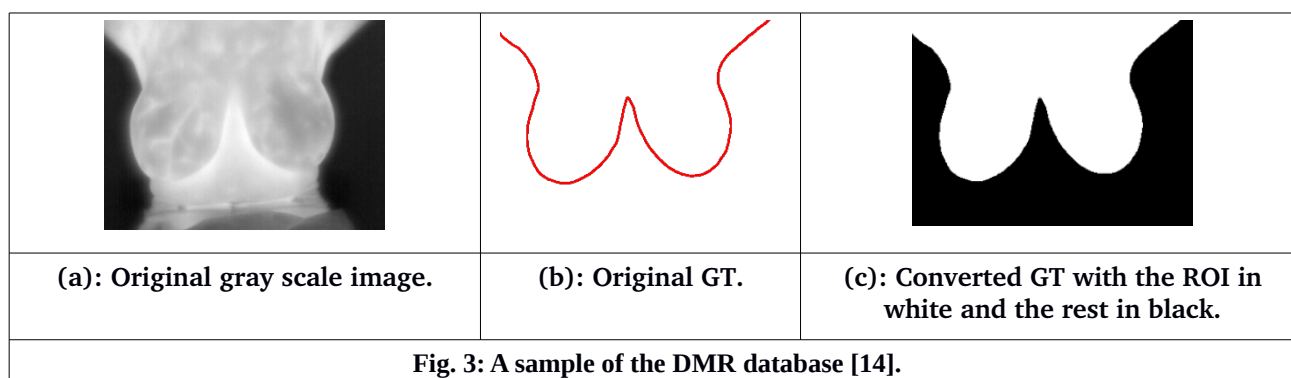
3.3. The Segmentation stage

Recovers spatial information, enables precise localization, and processing the concatenated feature maps, convoluted with a 1×1 filter kernel (customized convolution layer) to map them into two score maps, corresponding to ROI and Background (BG) classes in breast thermographic images. However, these score maps require to be aligned by segmentation scaling and cropping. The up-score layer, also known as deconvolution, performs nonlinear up-sampling to scale score maps, where the weights of the kernels of the up-sampling filter are initialized by bilinear interpolation [12]. Thereafter, a cropping layer will perform the cropping operation to remove any extends of the up-sampled feature maps, according to reference dimension provided by skip-connections (reference layer used to determine the size, height width, of the cropped output). Skip-connection performs a fully recover of the fine-grained spatial information lost in the convolution stage. Subsequently, the output cropping feature map is with the same resolution of the original image and having the combining context (local and global) with spatial information. In this work, The customized convolution, deconvolution, and cropping layers will be referred to as Fully Conventional block (FConv.). To perform pixel-wise classify, the softmax classifier layer is utilized to give the max probability that each pixel belongs to one of the classes. Lastly, followed by pixel classification layer which provides a categorical per-pixel label (ROI or BG) in the output segmentation image.

4. Experiments

4.1. Materials

In this work, the DMR database is utilized to evaluate the proposed augmentation segmentation technique. The DMR database is a public breast infrared thermographic mages database [13] and could be accessed online in [23]. The acquisition of the DMR database [14] is established by a FLIR SC-620 infrared camera with a resolution of 640×480 pixels, it has a thermal sensitivity less than $0.04 \text{ }^\circ\text{C}$ with a detectable temperature range between $-40 \text{ }^\circ\text{C}$ and $500 \text{ }^\circ\text{C}$. This database includes breast images of different shapes and sizes. The DMR database contains 285 frontal breast infrared thermographic gray-scale images as well as its ground truths (GT). The GTs images only have the contour of the ROI in red and the rest of the image in white. In this work, original GT images will be converted to black and white mask images by assigning index 0 to represent the black background pixels, and index 1 to represent the white ROI pixels. A sample of the data is seen in Figure 3.



4.2. Data Augmentation

In this work, two transformation approaches were utilized for data augmentation:

4.1.1. **The NSCT transformation:** The NSCT bands are employed as the model input, as mentioned before.

4.1.2. **The affine transformations:** A horizontal mirroring and shifting in width and height are two transformations to be used to augment the two image sets of the NSCT sub-bands (LB and HB). Firstly, the Horizontal Mirror transformation approach was used because the two breasts of a human are supposed to be symmetric around the vertical axis. Secondly, the shifting approach was used to produce translation invariance for the model; this approach is applied with a fraction of the total width or height of the image. Thus, the displacement of the images will be in nine different locations (top-left, top-centre, top-right, centre-left, centre-centre, center-right, bottom-left, bottom-centre and bottom-right).

4.2 . Training

The dataset was divided into 80% as the training set, 10% as validation set and 10% as the testing set. Then, these sets are passed to the pre-processing stage (the NSCT decomposition). The pre-processing stage boosts also the data augmentation. After that, the affine transformation of mirroring and shifting was applied only on the training set.

The proposed MBMP-FCN was trained using stochastic gradient descent (SGD) with learning rates of 10^{-4} , 60 epochs with a dropout rate of 33% and a momentum of 0.9. Moreover, a batch size of 22 and a validation frequency of 10.

4.3 . Computation Tools

The experiments were conducted on Deep Learning GPU Training System. The loading of the pre-trained model, fine-tuning, training and testing the model was carried through MATLAB version 2018. The training step of the proposed MPMB-FCN needs a good capacity of processing Parallel Computing Toolbox™ and a CUDA enabled NVIDIA GPU with a computation capability of 3.0. So this work uses a GPU NVIDIA Geforce GTX 1060 @ 6GB, computation capability of 6.1 and CUDA Toolkit Version of 9, on Ubuntu 16.04 LTS operating system. Only the training is costly for net execution. Once the training is performed, lower specification hardware is used for testing, an Intel Core i7-7500U CPU @ 2.70GHz × 4 and 16Gb of RAM in Ubuntu 16.04 LTS operating system as well.

5 .Experimental Results and Discussion

5.1 . Augmentation of the DMR database images

Table (1) gives the number of images after dividing the DMR database for training, validation, and testing sets. It shows the numbers of the LB and the HB images for the NSCT augmentation as well as the affine transformation augmentation. Eventually, Table (1) shows the total size of input images for the proposed MBMP-FCN. It is worth to note that the introduced data augmentation techniques enlarge the training set by approximately 54 times of the original training set.

Table 1: The total size of images after introduction of the augmentation approaches.

Set	Testing		Validation		Training	
DMR-IR dataset (285 images)	28 images (10%)		28 images (10%)		229 images (80%)	
Augmentation with NSCT Decomposition	LB	HB	LB	HB	LB	HB
	28*3= 84 images	28*3= 84 images	28*3= 84 images	28*3= 84 images	229*3= 687 images	229*3= 687 images
Augmentation with affine transformations	X-direction Mirroring				687*2= 1374 images	687*2= 1374 images
	X-direction transition in 3 positions				1374*3= 4122 images	1374*3= 4122 images
	Y-direction transition in 3 positions				4122*3= 12,366 images	4122*3= 12,366 images
The total number for training inputs					12,366 images	12,366 images

5.2 . Performance evaluation of the proposed MBMP-FCN

In this section, a set of experiments have been carried out assess the proposed method considering:

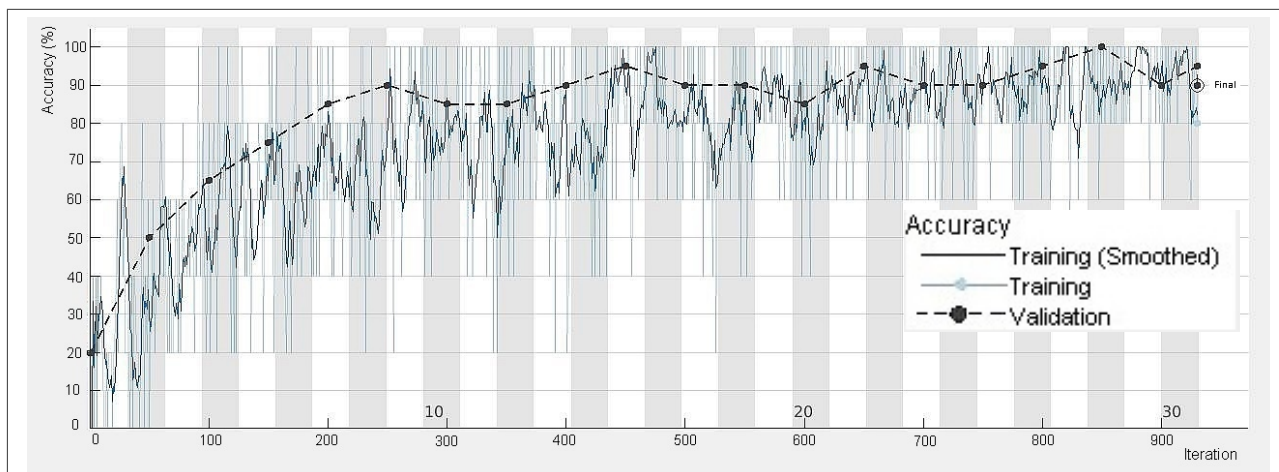
Segmentation influence: To evaluate the influence of the proposed MBMP-FCN is compared with its two paths as separated networks; i.e the High Band Fully Convolutional Network (HB-FCN) and the Low Band Fully Convolutional Network (LB-FCN). The LB-FCN is trained on the LB images of the NSCT which are the approximation components of the smooth and sub-sampled version of the original images. Therefore, most of the source images information is kept in low-frequency bands. In which those images allow local features to be learned, but limit the amount of global context that can be learned. The HB-FCN is trained on the HB images of the NSCT which contain the edges, contours representation, and texture features. The HB images will help the proposed network to learn more about the global context. Table (2) shows that the HB-FCN gave a weakly performance and the LB-FCN showed slightly higher performance in terms of training accuracy. In

contrast, the proposed MBMP-FCN out-performed the other models and achieved the state-of-the-art training accuracy of 99.22%.

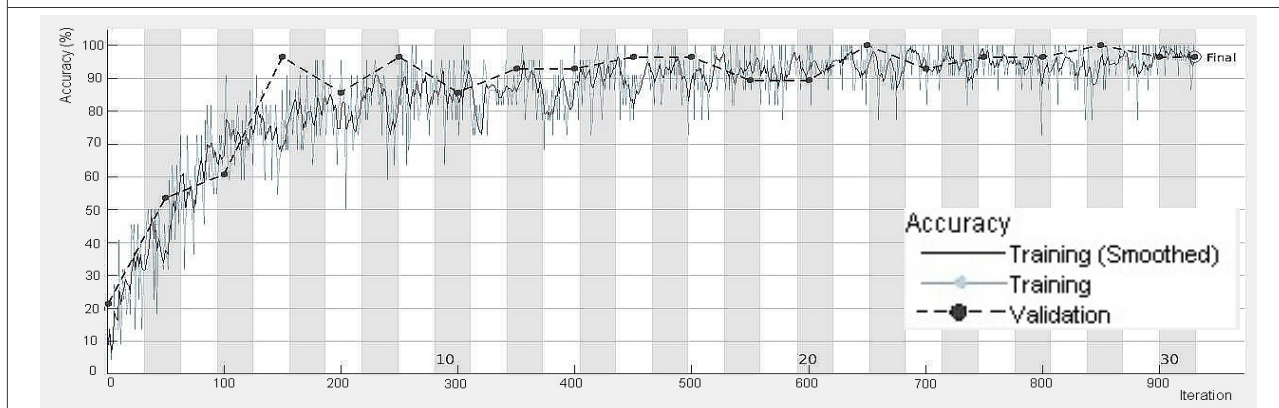
Table 2: Evaluation of the training accuracies for LB-FCN, HB-FCN, and MBMP-FCN.

Model	LB-FCN	HB-FCN	MBMP-FCN
Accuracy of training	95.45 %	81.02 %	99.22 %

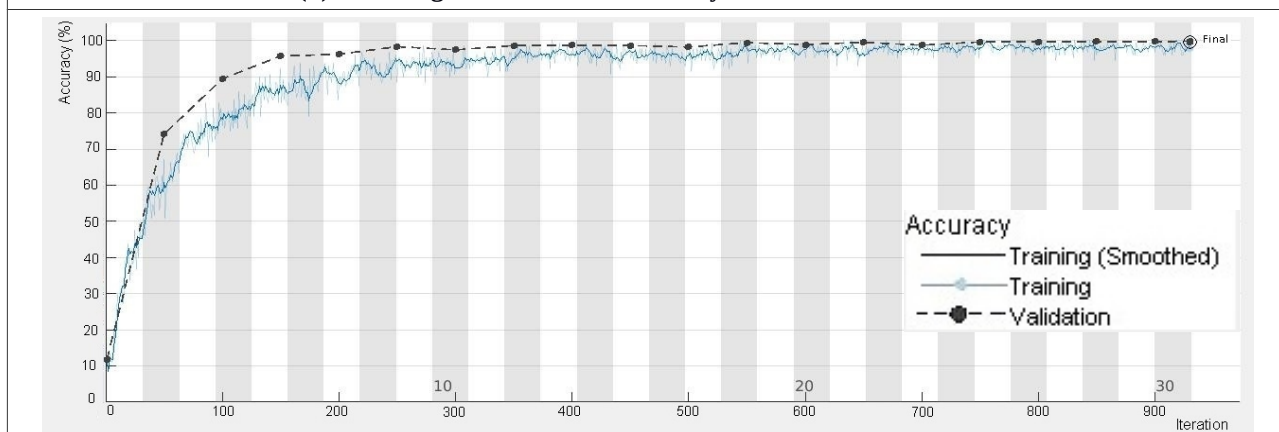
The corresponding training and validation accuracy curves for the MBMP-FCN are illustrated in Figure 4.



(a): Training and validation accuracy curves for the HB-FCN.



(b): Training and validation accuracy curves for the LB-FCN.

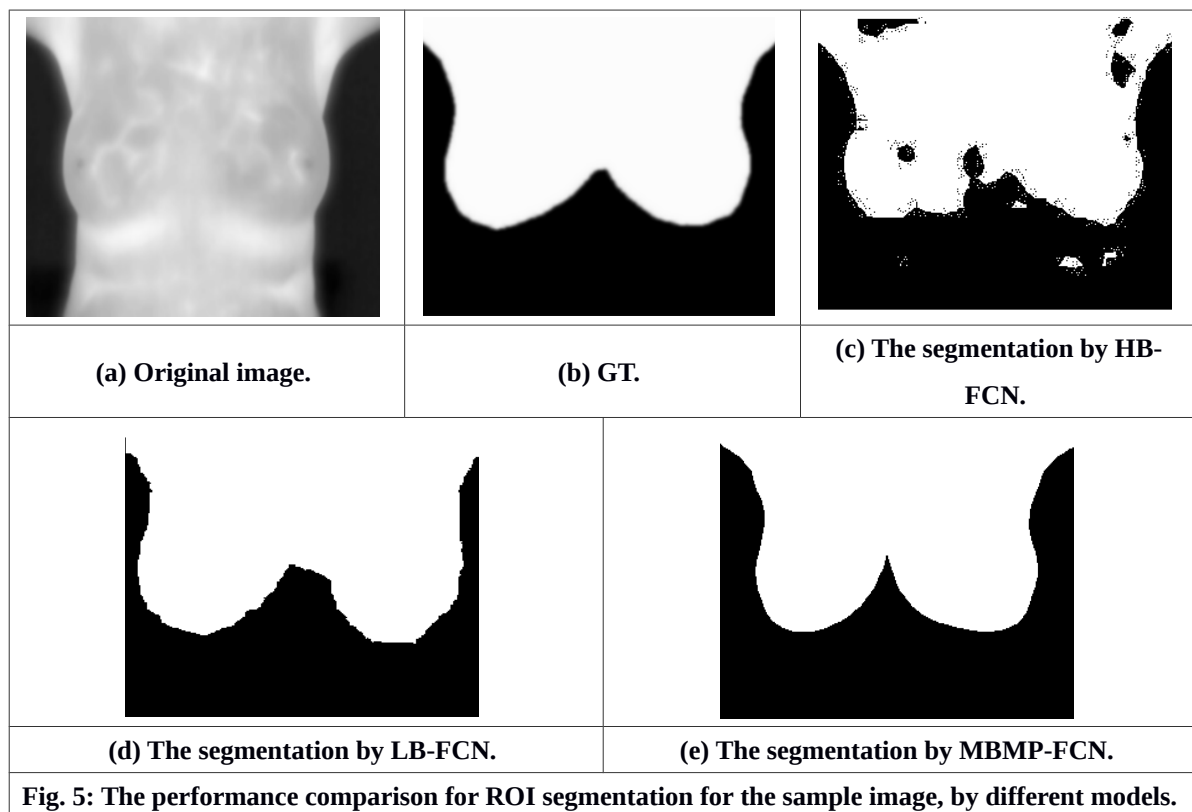


(c): Training and validation accuracy curves for the MBMP-FCN.

Fig. 4: Training and validation accuracy curves.

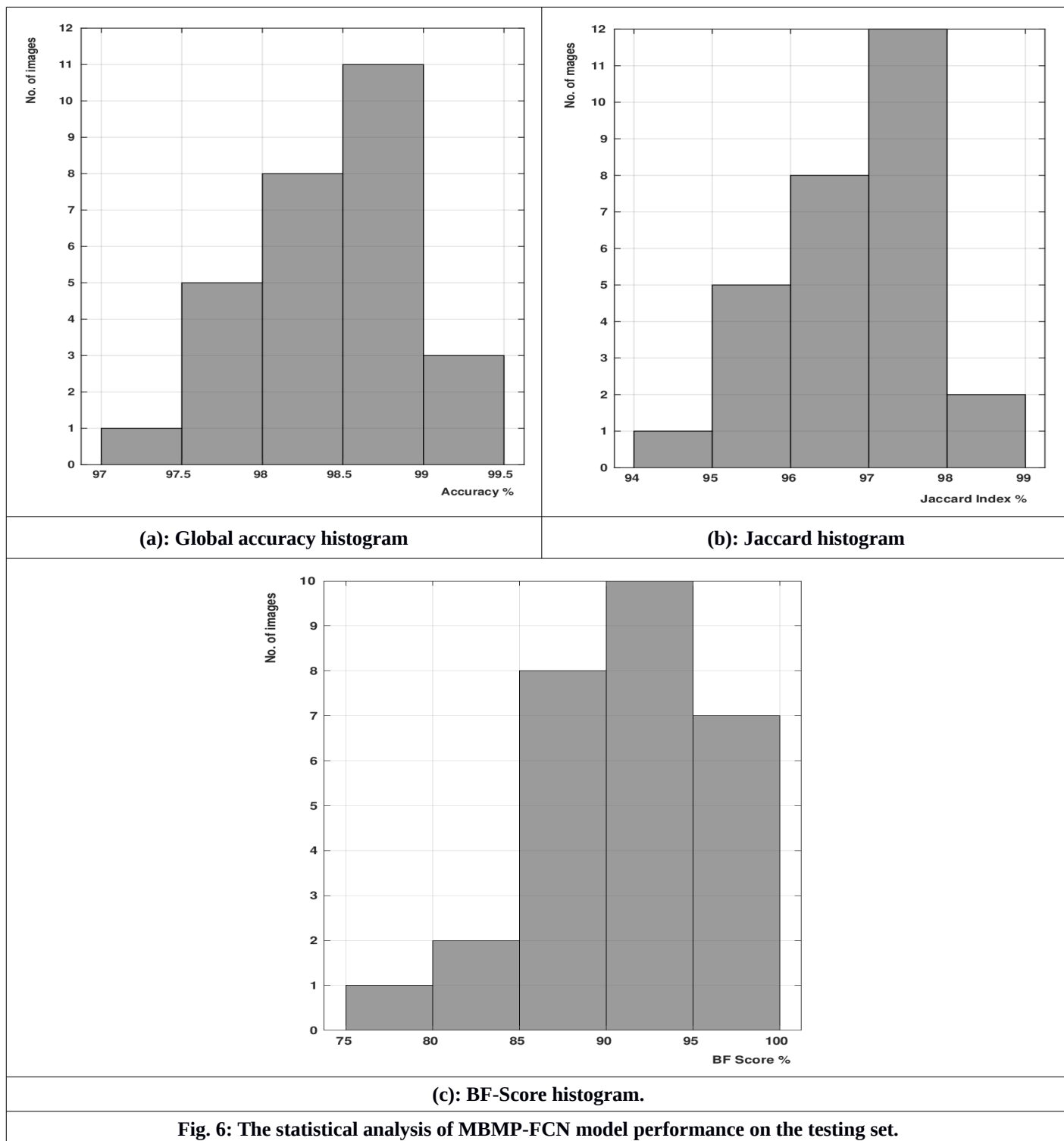
For the output the HB-FCN segmentation shown in Figure 5 (c), some little islands were wrongly identified. Those small areas are pixels that misclassified; as its features were discriminative by the network wrongly. Those areas mainly appear near the breast lower border that displays relatively higher confusion. In contrast, the observed boundaries were slightly smoother and less rough. For the output the LB-FCN segmentation

shown in Figure 5 (d), the model was able to estimate the presence and the rough position of ROI, except for the breast's boundary that was not smoothly delineated, while all pixels were correctly classified and efficiently prohibit the clutter of pixels in the background, and also better than the HB-FCN. That is because the HB-FCN was shorthanded of local contextual information in favor of HB information; similarly, the LB-FCN was shorthanded from the global knowledge in favor of local context. So, the combining of the learned features from LB-FCN and HB-FCN eliminates the necessity of choosing between global contextual information and precise boundary detail. Moreover, concatenating them allows information learned by both models to be exploited. Thus, from here emanated the need for multi paths with different inputs as in the proposed MBMP-FCN, to solve the fine-grained localization problem, accordingly, the proposal is yielding accurate semantic segmentation with well-recovered boundaries and delineated as observed in Figure 5 (e). In the proposed MBMP-FCN; it could be considered that HB-FCN and LB-FCN act as models that are mutually enhancing. The visualization results obtained from LB-FCN (before applying HB-FCN) already yields the breast pixels classification, while the addendum employing the HB-FCN further improves the performance by removing false classifications and refining the boundaries.



- **Assessment quantities:**

The second aspect is the assessment for the discriminative power of the proposed MBMP-FCN to perform the overall segmentation over the test set: Each ROI image in the test set will be evaluated whether the achieved output is in line with the GT or not. Three assessment quantities (Accuracy, Jaccard Index, and BF Score) are computed for each image in the test set. The histogram for each assessment quantity is illustrated in Figure 6.



As seen in Figure 6(a), most images, which present 78.6 % of the test set, have state-of-the-art accuracy by 98-99.5 %, which ensures the capability of the network to distinguish between BG and ROI pixels. As seen in Figure 6(b), the great majority of images by the percentage of 78.6 % of the test set scored 96-99% of Jaccard index and thus, the network could provide ROIs very similar to the delineation manually done by specialists. As seen in Figure 6(c), a percentage of 60.7% of images accomplished BF Score from 90 to 100% and 28.6% of images achieved 85-90%. So, the proposed MBMP-FCN achieved the refinement of the ROI Contour. Accordingly, the model was able to localize the ROI at the highest possible spatial precision of the boundaries delineation.

- **Visual quality**

The third aspect in this evaluation was the visual quality of a selected image sample of ROI segmented by the proposed MBMP-FCN, that could be obviously observed in Figure 7 and Table (3), which are the segmentation performance result and its differences to GT. For a more clear comparison, overlapped images between both GT and SEG images were generated.

Table 3: The visual evaluation of the proposed MBMP-FCN for segmenting the IR_5763

Measure	Accuracy	Jaccard index	BF Score
Value	99.1%	98.15%	98.78%

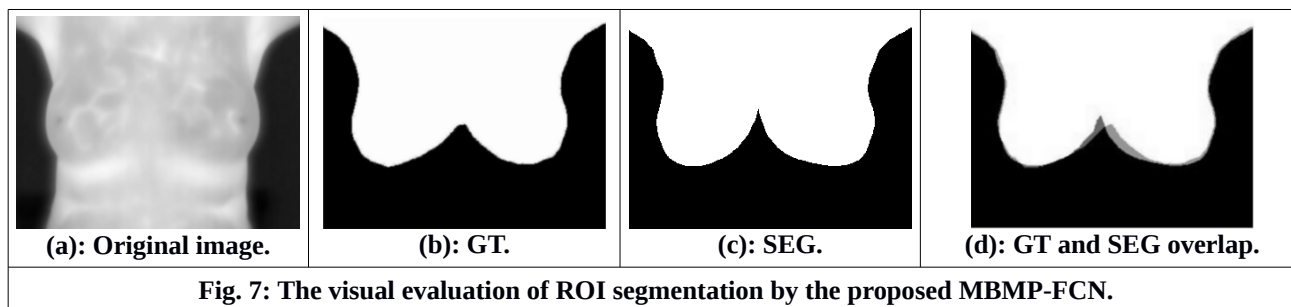


Fig. 7: The visual evaluation of ROI segmentation by the proposed MBMP-FCN.

The proposed MBMP-FCN produces a reasonable segmentation that could be easily observed at overlapped images. Also, the problem of intensity inhomogeneity of medical images; which is obvious in grey-scale breast thermographic image shown in Figure 7 (a); was resolved by the proposed model. Many images of breast thermography have large artifacts near the borders and edges. Consequently, what the true segmentation should include for these cases is not clear. On the other hand, the segmentation issue is manifested in identifying boundaries between ROI and the background, and boundaries of the lower edge of the patient's breasts, also those boundaries are with amorphous nature and unobvious limits. Whereas the proposed MBMP-FCN is ideal to handle these artifacts and achieves excellent performance as presented in Table (3).

• **Pixel classification**

The fourth aspect of assessing the performance is the ability of the proposed MBMP-FCN to correctly classify each pixel in the testing set either ROI or BG. The semantic segmentation could be considered as a classification task to classify each pixel in the image, therefore, the common performance metrics for classification will be used for this segmentation evaluation. That evaluation will be in terms of accuracy, sensitivity, and specificity as presented in Table (4). These results indicated that the proposed MBMP-FCN successfully segmented and correctly recognized the ROI as the model conducted excellent sensitivity. On the other hand, the model performed well in regards to the overall segmentation task and to classify the pixels of the background.

For further evaluation, an appropriate comparison among the proposed model and other techniques that used the same DMR database is established in Table (4). Results showed that the proposed MBMP-FCN had an excellent performance, providing ROI with higher accuracy. The comparison results are promising since no feature engineering was extracted, an automated end-to-end technique was accomplished and a state-of-the-art performance was achieved, despite the DMR dataset has an insufficient number of images for the general idea of deep networks.

Table 4: Comparison with the related DMR database.

Model parameter	Marques [15]	Motta [16]	AlexNet-FCN [11]	MBMP-FCN
Accuracy	97%	96%	97.99%	98.48%
Sensitivity	97%	88%	98.36%	99.4%
Specificity	97%	99%	97.61%	97.6%

The hand-crafted techniques have many limitations. Concerning Motta's method, it had ignored the upper quadrant part of breast, where there is a possibility of cancer incidence. Also, that method did not include clusters of lymphatic nodes in the axilla regions, above the collarbone, and in the chest, where the tumor, in many cases, is starting, so those regions are recommended to be included in the ROI image by some medical specialists concerned with thermal analysis. Unfortunately, the Motta method for segmentation was established by considering a rectangular area for ROI which is considered not efficient in the computer

science field. Unlike many previous methods, the proposed MBMP-FCN was able to include these regions in ROI.

• **Assessment of the segmented contour:**

Accordingly, A comparison was established between AlexNet-FCN [11] and the proposed MBMP-FCN for segmentation of breast infrared thermographic images. The BF Score evaluation is presented in Table (5). These metrics depicts how close the segmented thermographic images boundaries match the GT boundaries. It is obvious in Figure 8(b) that the ROI boundaries are conveniently reconstructed by the proposed MBMP-FCN. On the other hand, the ROI mask by AlexNet-FCN in Figure 8(c) suffers from rough and coarse edges. That signifies that the proposed MBMP-FCN has achieved the success to fetch both local and global context to produce a dense prediction with a smoother boundary of the breast area. Consequently, the existing intrinsic segmentation issue was tackled.

Table 5: Comparison of BF Score for the MBMP-FCN with AlexNet-FCN.

Model Parameter	AlexNet-FCN [11]	MBMP-FCN
Accuracy	97.99%	98.47%
Sensitivity	98.3%	98.4%
Specificity	97.61%	97.6%
Mean BF Score	85.58%	91.6 %

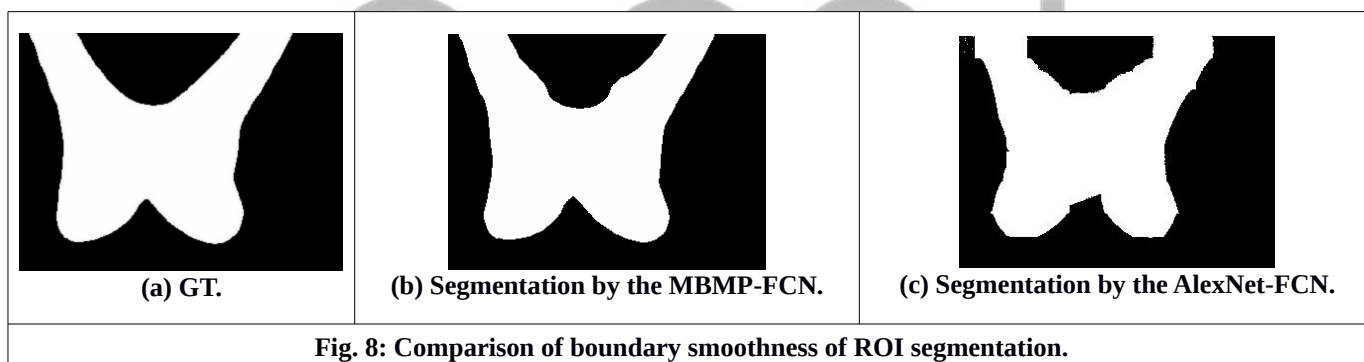


Fig. 8: Comparison of boundary smoothness of ROI segmentation.

5. Conclusion

The segmentation of a ROI in breast infrared thermographic images is a tough problem, as it is time-consuming and tedious work. As well, the refined and automated segmentation is required for CAD system of huge breast thermographic images. A proposed MBMP-FCN model was introduced in this work to resolve the rough segmentation issue that intrinsically exists in FCN based models. The proposed MBMP-FCN overcame this issue. Firstly by adding a sensitive preprocessing stage to feed the network with contours lpocal and global information. Secondly, revising the entire network architecture, the proposed model composed of two parallel-connected pre-trained FCN-AlexNets activated by the NSCT LB and HB bands learning different scales of features in the thermographic images. Then the two band features were concatenated to let the network be aware of position and fine shape of the ROI. The pre-trained network provides an auxiliary information that is greatly helpful for detecting objects pixel-wise showing high accuracy, specificity and sensitivity performance. Therefore, the proposed preprocessing two-path approach is more efficient and has a medium computational complexity. All of that allows for efficient and reliable regional analysis on large-scale datasets both in the clinic and in the research field.

References

- [1] A. Mert, N. Kılıç, E. Bilgili, and A. Akan, “Breast cancer detection with reduced feature set,” *Comput. Math. Methods Med.*, vol. 2015, 2015.
- [2] B. Krawczyk, G. Schaefer, and M. Wozniak, “Combining one-class classifiers for imbalanced classification of breast thermogram features,” in *2013 Fourth International Workshop on Computational Intelligence in Medical Imaging (CIMI)*, 2013, pp. 36–41.
- [3] E.-K. Ng, “A review of thermography as promising non-invasive detection modality for breast tumor,” *Int. J. Therm. Sci.*, vol. 48, no. 5, pp. 849–859, 2009.
- [4] M. Gautherie and C. M. Gros, “Breast thermography and cancer risk prediction,” *Cancer*, vol. 45, no. 1, pp. 51–56, 1980.
- [5] E. Y. K. Ng and E. C. Kee, “Integrative computer-aided diagnostic with breast thermogram,” *J. Mech. Med. Biol.*, vol. 7, no. 01, pp. 1–10, 2007.
- [6] J. R. Keyserlingk, P. D. Ahlgren, E. Yu, and N. Belliveau, “Infrared Imaging of the Breast: Initial Reappraisal Using High-Resolution Digital Technology in 100 Successive Cases of Stage I and II Breast Cancer,” *Breast J.*, vol. 4, no. 4, pp. 245–251, 1998.
- [7] T. Gaber *et al.*, “Thermogram breast cancer prediction approach based on Neutrosophic sets and fuzzy c-means algorithm,” in *2015 37th Annual International Conference of the IEEE Engineering in Medicine and Biology Society (EMBC)*, 2015, pp. 4254–4257.
- [8] A. M. Chiarelli *et al.*, “Digital versus screen-film mammography: impact of mammographic density and hormone therapy on breast cancer detection,” *Breast Cancer Res. Treat.*, vol. 154, no. 2, pp. 377–387, 2015.
- [9] T. B. Borchardt, A. Conci, R. C. F. Lima, R. Resmini, and A. Sanchez, “Breast thermography from an image processing viewpoint: A survey,” *Signal Processing*, vol. 93, pp. 2785–2803, 2013, doi: 10.1016/j.sigpro.2012.08.012.
- [10] M. N. Do and M. Vetterli, “The contourlet transform: an efficient directional multiresolution image representation,” *IEEE Trans. Image Process.*, vol. 14, no. 12, pp. 2091–2106, 2005.
- [11] M. B. T. and A. M. Elbagoury*, “Breast Infrared Thermography Segmentation Based on Adaptive Tuning of a Fully Convolutional Network,” *Current Medical Imaging*, vol. 16, no. 5, pp. 611–621, 2020, doi: <http://dx.doi.org/10.2174/1573405615666190503142031>.
- [12] D. T. Long J, Shelhamer E, “Fully Convolutional Networks for Semantic Segmentation,” *Proc. IEEE Conf. Comput. Vis. Pattern Recognit. - CVPR '15*, vol. 1, no. 1, pp. 3431–3440, Nov. 2015, doi: 10.1007/978-981-10-3147-2.
- [13] L. F. Silva *et al.*, “A New Database for Breast Research with Infrared Image,” *J. Med. Imaging Heal. Informatics*, vol. 4, no. 1, pp. 92–100, 2014, doi: 10.1166/jmihi.2014.1226.
- [14] “DMR, Visual Lab. Database for mastology research. <http://visual.ic.uff.br/dmi/>, 2017.”
- [15] R. S. Marques, “Segmentação automática das mamas em imagens térmicas,” *Master’s thesis, Inst. Comput. Univ. Fed. Flum. Niterói, RJ, Bras.*, 2012.
- [16] L. S. Motta, “Obtenção automática da região de interesse em termogramas frontais da mama para o auxílio à detecção precoce de doenças,” *M Sc. Diss. (in Port. Comput. Institute. UFF, Niteroi, Brazil)*, 2010.